Gravitational radiation from a particle plunging into a Schwarzschild black hole: Frequency-domain and semirelativistic analyses

Hector O. Silva[1], Giovanni Tambalo[1], Kostas Glampedakis[2,3] and Kent Yagi[4]

[1]*Max Planck Institute for Gravitational Physics (Albert Einstein Institute), D-14476 Potsdam, Germany*
[2]*Departamento de Física, Universidad de Murcia, Murcia, E-30100, Spain*
[3]*Theoretical Astrophysics, University of Tübingen, Auf der Morgenstelle 10, D-72076 Tübingen, Germany*
[4]*Department of Physics, University of Virginia, Charlottesville, Virginia 22904, USA*

We revisit the classic problem of gravitational wave emission by a test particle plunging into a Schwarzschild black hole both in the frequency-domain Regge-Wheeler-Zerilli formalism and in the semirelativistic approximation. We use, and generalize, a transformation due to Nakamura, Sasaki, and Shibata to improve the falloff of the source term of the Zerilli function. The faster decay improves the numerical convergence of quantities of interest, such as the energy radiated at spatial infinity through gravitational waves. As a test of the method, we study the gravitational radiation produced by test particles that plunge into the black hole with impact parameters close to the threshold for scattering. We recover and expand upon previous results that were obtained using the Sasaki-Nakamura equation. In particular, we study the relative contributions to the total energy radiated due to waves of axial and polar parity, and uncover an universal behavior in the waveforms at late times. We complement our study with a semirelativistic analysis of the problem, and we compare the two approaches. The generalized Nakamura-Sasaki-Shibata transformation presented here is a simple and practical alternative for the analysis of gravitational-wave emission by unbound orbits in the Schwarzschild spacetime using the frequency-domain Regge-Wheeler-Zerilli formalism.

I. INTRODUCTION

The study of gravitational radiation produced by test particles in black-hole spacetimes has a long history dating back to the early 1970s, and played a central role in the early development of the understanding of potential gravitational-wave sources [1,2]. In the framework of black-hole perturbation theory, developed by Regge *et al.* [3,4], the pioneering works on this problem were done by Zerilli [5], Davies *et al.* [6–8], Chung [9], and Ruffini [10]. These works assumed particles in unbound trajectories that start from spatial infinity and plunge into a Schwarzschild black hole.

Critical to these calculations is the asymptotic behavior of the source term that encapsulates how the test particle excites the gravitational perturbations. As an extreme example, the source term of the Teukolsky equation, that describes the gravitational perturbations of a Kerr black hole [11], diverges at spatial infinity for unbound geodesics. In principle, this jeopardizes the calculation of

physical quantities of interest, such as gravitational waveforms or the energy carried away to infinity by the waves. To circumvent this problem, one can either develop a regularization scheme [12–15], or rewrite the Teukolsky equation to tame the source's asymptotic behavior. Pursuing the latter approach, Sasaki and Nakamura [16–18] found their eponymous equation, widely used in the study of unbound geodesics both in Schwarzschild and Kerr spacetimes; see, e.g., Refs. [19–24], respectively, for early work. A somewhat similar situation also happens when the perturbations of a Schwarzschild black hole are described in terms of the Cunningham-Price-Moncrief [25] and Zerilli-Moncrief [26] functions. Less dramatically, the source term of the Zerilli equation has a slow falloff at spatial infinity. See Hopper [27] for a detailed discussion.

In a serendipitous event, in the course of a related investigation, we learned of a work by Shibata and Nakamura that presents a simple transformation of the Zerilli function to improve the falloff of the source term of the Zerilli equation, and that was applied to the radial infall case only [28].[1] Here we revisit this method and extend its application range to problems involving particles plunging

---

[1]Reference [28] cites an unpublished work by Nakamura and Sasaki when introducing this transformation, that we will refer to as the Nakamura-Sasaki-Shibata transformation.

with nonzero angular momentum. This allows us to reexamine some aspects of the gravitational radiation produced by particles that plunge with angular momenta near the threshold for scattering. This situation is relevant in the context of understanding ultrarelativistic binary black hole collisions, and that was until now only studied in detail using the Sasaki-Nakamura equation; see Berti et al. [29] and references therein. We complement our study of this problem with a calculation of the energy radiated within the semirelativistic approximation of Ruffini and Sasaki [30].

This paper is organized as follows. In Sec. II, we review the motion of test particles plunging into a Schwarzschild black hole. In Sec. III, we provide a summary of Regge-Wheeler-Zerilli formalism and identify the main issue we want to resolve. In Sec. IV, we review and generalize the method of Ref. [28]. In Sec. V, we describe our numerical methods and present our numerical results. In Sec. VI, we compare our results against an analysis in the semi-relativistic approximation. We summarize our findings in Sec. VII. We use the mostly plus metric signature and use geometrical units with $c = G = 1$, unless stated otherwise.

II. GEODESIC MOTION

We consider a particle of mass μ in geodesic motion the spacetime of a Schwarzschild black hole of mass M, with $\mu/M \ll 1$. We use Schwarzschild-Droste coordinates $x^\mu = \{t, r, \theta, \phi\}$ in which the spacetime's line element is

$$ds^2 = -f(r)dt^2 + f^{-1}(r)dr^2 + r^2(d\theta^2 + \sin^2\theta d\phi^2), \quad (1)$$

where $f = 1 - 2M/r$ and $r = 2M$ is the location of the event horizon.

We assume that the particle starts from rest at infinity with (conserved) energy $\mathcal{E} = E/\mu = 1$ and angular momentum $\mathcal{L} = L/\mu$ per unit mass. If we chose, without loss of generality, that the particle's motion happens in the equatorial plane $\theta = \pi/2$, then we can parametrize the particle's worldline in terms of the proper time τ as $z^\mu(\tau) = \{t_p, r_p, \pi/2, \phi_p\}$, and, from the geodesic equation and the timelike constraint $g_{ab}u^a u^b = -1$, with $u^a = dz^a/dt$, we obtain

$$\dot{t}_p = \mathcal{E}/f_p, \quad \dot{\phi}_p = \mathcal{L}/r_p^2, \quad \dot{r}_p^2 = \mathcal{E}^2 - U(r_p, \mathcal{L}), \quad (2)$$

where $\dot{} = d/d\tau$ and

$$U = f(1 + \mathcal{L}^2/r^2), \quad (3)$$

is the effective radial potential.

The particle's trajectories are classified according to the number of real roots of $\mathcal{E}^2 - U$. For the special case $\mathcal{E} = 1$ the analysis is simple, and we find the roots to be
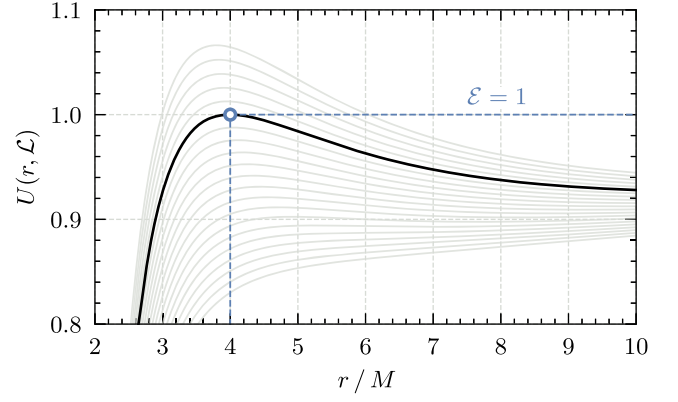

FIG. 1. The effective potential $U(r, \mathcal{L})$ for various values of $\mathcal{L}$, which ranges from $3.25M$ (lowermost solid gray line) to $4.25M$ (uppermost solid gray line). For a particle falling from rest from infinity ($\mathcal{E} = 1$) into the hole, there is a critical value of $\mathcal{L}_{\text{crit}} = 4M$ (solid black line) for which the particle becomes trapped in a marginally stable circular orbit at $r = 4M$. This value of $\mathcal{L}$ separates plunging ($\mathcal{L} < \mathcal{L}_{\text{crit}}$) from scattering ($\mathcal{L} > \mathcal{L}_{\text{crit}}$) geodesics.

$$r_\pm = \frac{\mathcal{L}}{4M}[\mathcal{L} \pm (\mathcal{L}^2 - 16M^2)^{1/2}]. \quad (4)$$

Hence, a plunging orbit from infinity requires that $\mathcal{L} < 4M$, for otherwise the turning points are real and positive (i.e., the particle is scattered). We will define this special value of the angular momentum as $\mathcal{L}_{\text{crit}} = 4M$.

In Fig. 1 we show the effective potential (3) for a range of values $\mathcal{L}/M \in \{3.25, 4.25\}$ (light curves). The thicker line corresponds to $U(r, \mathcal{L}_{\text{crit}})$, which peaks at $r = 4M$ with a value of 1. Hence, a particle falling from rest and with angular momentum $\mathcal{L} = \mathcal{L}_{\text{crit}}$ will be captured in a marginally stable circular orbit. A particle with $\mathcal{L}$ larger (smaller) than $\mathcal{L}_{\text{crit}}$ will scatter (plunge).

It is convenient to rewrite Eq. (2) as first-order in r equations,

$$dt_p/dr_p = -(\mathcal{E}/f_p)(\mathcal{E}^2 - U_p)^{-1/2}, \quad (5a)$$

$$d\phi_p/dr_p = -(\mathcal{L}/r_p^2)(\mathcal{E}^2 - U_p)^{-1/2}, \quad (5b)$$

where we have taken $\dot{r}_p < 0$. We integrate Eq. (5) with initial conditions $t_p(r_{\text{max}}) = 0$ and $\phi_p(r_{\text{max}}) = 0$ at some arbitrarily large $r_p = r_{\text{max}}$ down to the horizon, $r_p = 2M$. In Fig. 2 we show a sequence of trajectories starting from $\mathcal{L}/M = 3.25$ and up to $\mathcal{L}/M = 3.9996$ (i.e., with 99.99% of $\mathcal{L}_{\text{crit}}$). We translate from Schwarzschild-Droste to Cartesian coordinates using

$$x_p = r_p \cos\phi_p, \quad y_p = r_p \sin\phi_p, \quad z_p = 0. \quad (6)$$
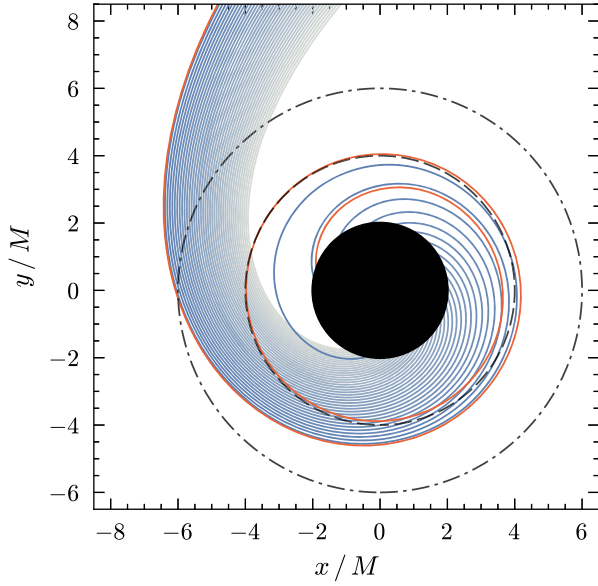
FIG. 2. Timelike geodesics with angular momentum per unit mass $\mathcal{L}/M \in \{3.25, 3.9996\}$ plunging into a Schwarzschild black hole (black disk) starting from rest at spatial infinity, $\mathcal{E} = 1$. The dot-dashed line represents to the innermost stable circular orbit ($r = 6M$) and the dashed line corresponds to the location of the marginally stable circular orbit ($r = 4M$). In the limit $\mathcal{L}/\mathcal{L}_{\text{crit}} \to 1$, the particle executes an increasing fractional number of orbits $\phi/(2\pi)$, as seen in the red curve that corresponds to $\mathcal{L} = 3.9996M$, or 99.99% of $\mathcal{L}_{\text{crit}}$.

As the ratio $\mathcal{L}/\mathcal{L}_{\text{crit}}$ approaches unity from below, the particle executes an increasing fractional number of orbits $\phi_p/(2\pi)$, given approximately by $-(\sqrt{2}\pi)^{-1}\log(1 - \mathcal{L}/\mathcal{L}_{\text{crit}})$ [31].

III. BLACK HOLE PERTURBATIONS IN THE REGGE-WHEELER-ZERILLI GAUGE

We are interested in calculating the gravitational waves produced by a particle plunging in a Schwarzschild black hole. The standard treatment of this problem, in the metric-perturbation formalism, is due to Regge and Wheeler [3] and Zerilli [4,5]. The problem reduces to solving two equations in the time domain:

$$\left[-\frac{\partial^2}{\partial t^2} + \frac{\partial^2}{\partial x^2} - V_\ell^{(\pm)}(r) \right] X_{\ell m}^{(\pm)}(t, r) = S_{\ell m}^{(\pm)}(t, r), \quad (7)$$

or, by going to the Fourier domain, through

$$X_{\ell m}^{(\pm)}(t, r) = \frac{1}{2\pi} \int_{-\infty}^{\infty} d\omega\, e^{-i\omega t} X_{\ell m \omega}^{(\pm)}(r), \quad (8)$$

we have alternatively

$$\left[\frac{d^2}{dx^2} + \omega^2 - V_\ell^{(\pm)}(r) \right] X_{\ell m \omega}^{(\pm)}(r) = S_{\ell m \omega}^{(\pm)}(r). \quad (9)$$

In these equations, x is the tortoise coordinate

$$x = r + 2M \log[r/(2M) - 1] \quad (10)$$

that maps the region $2M < r < \infty$ to $-\infty < x < \infty$. The superscript $(\pm)$ denotes variables associated to metric perturbations of polar $(+)$ or axial $(-)$ parity, and $V_\ell^{(\pm)}$ is an effective potential. Perturbations of each parity are described by a single master function, known as the Zerilli $X^{(+)}$ and Regge-Wheeler $X^{(-)}$ functions, respectively. The effective potentials associated to each of these perturbations bear the same respective names and are given by

$$V_\ell^{(+)} = \frac{f}{r^2 \Lambda^2} \left[2\lambda^2(\Lambda + 1) + \frac{18M^2}{r^2}\left(\lambda + \frac{M}{r}\right) \right], \quad (11a)$$

$$V_\ell^{(-)} = \frac{f}{r^2}\left[\ell(\ell + 1) - \frac{6M}{r} \right], \quad (11b)$$

where we defined

$$\lambda = (\ell + 2)(\ell - 1)/2 \quad \text{and} \quad \Lambda = \lambda + 3M/r. \quad (12)$$

The function $S_{\ell m \omega}^{(\pm)}$ is the source term, responsible for the excitation of the gravitational perturbations. A detailed derivation of this source term in the Regge-Wheeler-Zerilli formalism can be found, e.g., in Refs. [32,33], whose results we quote in Appendix A.

Because the potential $V_\ell^{(\pm)}$ vanishes both at the horizon and at infinity, and provided that the source vanishes sufficiently fast at both boundaries, the solutions to Eq. (7) can be written as plane waves for $x \to \pm\infty$. We will impose that $X_{\ell m \omega}^{(\pm)}$ is purely ingoing at the event horizon and purely outgoing at spatial infinity, that is,

$$X_{\ell m \omega}^{(\pm)} \simeq \begin{cases} C_{\ell m \omega}^{(\pm),\,\text{in}} e^{-i\omega x} & x \to -\infty \\ C_{\ell m \omega}^{(\pm),\,\text{out}} e^{+i\omega x} & x \to +\infty \end{cases}. \quad (13)$$

To solve the inhomogeneous differential equation (7), we use the method of variation of parameters. The method consists of finding two linearly independent solutions, say $X_{\ell m \omega}^{(\pm),\,\text{in}}$ and $X_{\ell m \omega}^{(\pm),\,\text{up}}$, of the homogeneous equations

$$\left[\frac{d^2}{dx^2} + \omega^2 - V_\ell^{(\pm)}(r) \right] X_{\ell m \omega}^{(\pm),\,\text{up/in}} = 0. \quad (14)$$

The two solutions differ by the boundary conditions we impose when we solve Eq. (14), namely,

$$X_{\ell m \omega}^{(\pm),\,\text{in}} \simeq \begin{cases} e^{-i\omega x} & x \to -\infty \\ A_{\ell m \omega}^{(\pm),\,\text{in}} e^{-i\omega x} + A_{\ell m \omega}^{(\pm),\,\text{out}} e^{+i\omega x} & x \to +\infty \end{cases} \quad (15a)$$

$$X_{\ell m\omega}^{(\pm),\mathrm{up}} \simeq \begin{cases} B_{\ell m\omega}^{(\pm),\mathrm{in}} e^{-i\omega x} + B_{\ell m\omega}^{(\pm),\mathrm{out}} e^{+i\omega x} & x \to -\infty \\ e^{i\omega x} & x \to +\infty \end{cases}. \quad (15b)$$

We use these solutions to define the Wronskian,

$$W_{\ell m\omega}^{(\pm)} = X_{\ell m\omega}^{(\pm),\mathrm{in}} \frac{dX_{\ell m\omega}^{(\pm),\mathrm{up}}}{dx} - X_{\ell m\omega}^{(\pm),\mathrm{up}} \frac{dX_{\ell m\omega}^{(\pm),\mathrm{in}}}{dx}, \quad (16)$$

which is constant in x. We then construct the Green's function as

$$G_{\ell m\omega}^{(\pm)}(x,x') = \frac{1}{W_{\ell m\omega}^{(\pm)}} \Big[X_{\ell m\omega}^{(\pm),\mathrm{up}}(x) X_{\ell m\omega}^{(\pm),\mathrm{in}}(x') \Theta(x-x')$$
$$+ X_{\ell m\omega}^{(\pm),\mathrm{in}}(x) X_{\ell m\omega}^{(\pm),\mathrm{up}}(x') \Theta(x'-x) \Big], \quad (17)$$

where $\Theta(\cdot)$ is the Heaviside step function. Finally, with the Green's function (17), we can write the solution of Eq. (7) as

$$X_{\ell m\omega}^{(\pm)} = \frac{1}{W_{\ell m\omega}^{(\pm)}} \Big[X_{\ell m\omega}^{(\pm),\mathrm{up}} \int_{-\infty}^{x} dx' X_{\ell m\omega}^{(\pm),\mathrm{in}} S_{\ell m\omega}^{(\pm)}$$
$$+ X_{\ell m\omega}^{(\pm),\mathrm{in}} \int_{x}^{+\infty} dx' X_{\ell m\omega}^{(\pm),\mathrm{up}} S_{\ell m\omega}^{(\pm)} \Big]. \quad (18)$$

Equation (18) has the desired property of being purely ingoing at the horizon and purely outgoing at infinity:

$$\lim_{x \to -\infty} X_{\ell m\omega}^{(\pm)} \simeq \frac{e^{-i\omega x}}{W_{\ell m\omega}^{(\pm)}} \int_{-\infty}^{\infty} dx' X_{\ell m\omega}^{(\pm),\mathrm{up}} S_{\ell m\omega}^{(\pm)}, \quad (19a)$$

$$\lim_{x \to +\infty} X_{\ell m\omega}^{(\pm)} \simeq \frac{e^{+i\omega x}}{W_{\ell m\omega}^{(\pm)}} \int_{-\infty}^{\infty} dx' X_{\ell m\omega}^{(\pm),\mathrm{in}} S_{\ell m\omega}^{(\pm)}, \quad (19b)$$

where we used the boundary conditions on $X_{\ell m\omega}^{(\pm),\mathrm{up/in}}$.

We can compare Eq. (19b) with the boundary conditions Eq. (13) imposed on $X_{\ell m\omega}^{(\pm)}$, and make the identification,

$$C_{\ell m\omega}^{(\pm),\mathrm{out}} = \frac{1}{W_{\ell m\omega}^{(\pm)}} \int_{-\infty}^{+\infty} dx' X_{\ell m\omega}^{(\pm),\mathrm{in}} S_{\ell m\omega}^{(\pm)}. \quad (20)$$

This is the main quantity we must numerically calculate to obtain, e.g., the time-domain gravitational waveform or the energy radiated to infinity. More specifically, we will be interested in the spectral energy distribution in each (ℓ, m) mode

$$\frac{dE_{\ell m}}{d\omega} = \frac{\omega^2}{64\pi^2} \frac{(\ell+2)!}{(\ell-2)!} \Big[|C_{\ell m\omega}^{(+),\mathrm{out}}|^2 + \frac{4}{\omega^2} |C_{\ell m\omega}^{(-),\mathrm{out}}|^2 \Big], \quad (21)$$

and in the time-domain Regge-Wheeler and Zerilli mode functions

$$X_{\ell m}^{(\pm)}(t,x) = \frac{1}{2\pi} \int_{-\infty}^{+\infty} d\omega C_{\ell m\omega}^{(\pm),\mathrm{out}} e^{-i\omega(t-x)}. \quad (22)$$

In practice, we note that, as $x \to \infty$, the Wronskian becomes

$$W_{\ell m\omega}^{(\pm)} = 2i\omega A_{\ell m\omega}^{(\pm),\mathrm{in}}, \quad (23)$$

and that we can also rewrite Eq. (20) as

$$C_{\ell m\omega}^{(\pm),\mathrm{out}} = \frac{1}{W_{\ell m\omega}^{(\pm)}} \int_{2M}^{+\infty} \frac{dr'}{f} X_{\ell m\omega}^{(\pm),\mathrm{in}} S_{\ell m\omega}^{(\pm)}. \quad (24)$$

Because $f \simeq 1$ and $X_{\ell m\omega}^{(\pm),\mathrm{in}} \simeq \exp(\pm i\omega x)$ as $x \to \infty$, we see that the convergence of this integral depends critically on the asymptotic properties of $S_{\ell m\omega}^{(\pm)}$.

IV. ASYMPTOTIC BEHAVIOR OF THE FREQUENCY DOMAIN SOURCES

We now review the properties of $S_{\ell m\omega}^{(+)}$ in two cases of interest. We will start by reviewing the case in which the particle falls radially, $\mathcal{L} = 0$, into the black hole and how Ref. [28] improved the asymptotic behavior of $S_{\ell m\omega}^{(+)}$. We will then show one way in which the Nakamura-Sasaki-Shibata transformation can be generalized to general plunging trajectories, $\mathcal{L} \neq 0$, and discuss the asymptotic properties of this new source term.

A. The case of radial infall

When $\mathcal{L} = 0$, $S_{\ell m\omega}^{(-)}$ vanishes and $S_{\ell m\omega}^{(+)}$ simplifies to [6,7]

$$S_{\ell m\omega}^{(+)} = -8\pi\mu A_{\ell m} \frac{f}{r\Lambda} \Big[\sqrt{\frac{r}{2M}} - \frac{2i}{\omega} \frac{\lambda}{r\Lambda} \Big] e^{i\omega t_p(r)}, \quad (25)$$

where $A_{\ell m} = Y_{\ell m}^*(\pi/2, \phi) \exp(im\phi)$, $Y_{\ell m}$ are the spherical harmonics, the asterisk indicates complex conjugation, and t_p is given by

$$\frac{t_p}{2M} = -\frac{2}{3} \Big(\frac{r}{2M} \Big)^{\frac{3}{2}} - 2 \Big(\frac{r}{2M} \Big)^{\frac{1}{2}} + \log \Big[\frac{\sqrt{r/(2M)}+1}{\sqrt{r/(2M)}-1} \Big]. \quad (26)$$

We find that the near-horizon and spatial-infinity behaviors of $S_{\ell m\omega}^{(+)}$ are

$$S_{\ell m\omega}^{(+)} \simeq \begin{cases} 0 & x \to -\infty \\ x^{-1/2} & x \to +\infty \end{cases}. \quad (27)$$

Hence the integral Eq. (20) converges slowly at spatial infinity. To improve the convergence, Ref. [28] proposed the substitution[2]

---

[2]Our notation differs from that used in Ref. [28]. See also Ref. [13], for a similar substitution in the context of the Teukolsky equation.

$$X_{\ell m\omega}^{(+)} = \tilde{X}_{\ell m\omega}^{(+)} + Q_{\ell m\omega}, \qquad (28)$$

where

$$Q_{\ell m\omega} = -\frac{8\pi\mu\mathcal{A}_{\ell m}}{\omega^2}\frac{f}{r\Lambda}\sqrt{\frac{2M}{r}}e^{i\omega t_p}. \qquad (29)$$

The function $Q_{\ell m\omega}$ vanishes at the event horizon $x \to -\infty$ and decays as $x^{-3/2}$ for $x \to \infty$. Thus, $X_{\ell m\omega}^{(+)} \simeq \tilde{X}_{\ell m\omega}^{(+)}$ in the latter limit.

We then insert Eq. (28) in Eq. (7) to find

$$\left[\frac{d^2}{dx^2} + \omega^2 - V_\ell^{(+)}\right]\tilde{X}_{\ell m\omega}^{(+)} = \tilde{S}_{\ell m\omega}^{(+)}, \qquad (30)$$

where $\tilde{S}_{\ell m\omega}^{(+)}$ is a new source term given by

$$\tilde{S}_{\ell m\omega}^{(+)} = S_{\ell m\omega}^{(+)} - \left[\frac{d^2}{dx^2} + \omega^2 - V_\ell^{(+)}\right]Q_{\ell m\omega}. \qquad (31)$$

The asymptotic behaviors of the new source term are

$$\tilde{S}_{\ell m\omega}^{(+)} \simeq \begin{cases} 0 & x \to -\infty \\ x^{-3/2} & x \to +\infty \end{cases}, \qquad (32)$$

making the integral in Eq. (20) converge faster. One can verify that it is the second x derivative of $Q_{\ell m\omega}$ in Eq. (31) that yields a term that decays as $r^{-1/2}$ as $x \to \infty$, and that cancels the leading-order asymptotic term in the large-x expansion of the original source term. We note that both $X_{\ell m\omega}^{(+)}$ and $\tilde{X}_{\ell m\omega}^{(+)}$ satisfy the same homogeneous equation. Hence, we can calculate $C_{\ell m\omega}^{(\pm),\,\text{out}}$ with the mere replacement $S_{\ell m\omega}^{(+)} \to \tilde{S}_{\ell m\omega}^{(+)}$ in Eq. (24).

In Fig. 3, we show both the original (25) and the Nakamura-Sasaki-Shibata-transformed (31) source terms of the Zerilli equation for a particle falling radially into the black hole, and $\ell = m = 2$ and $M\omega = 0.3$. In the left panel we show their absolute values. In the right panels we show the real (solid line) and imaginary (dashed line) parts of the original (top panel) and new (bottom panel) source terms. The faster decay of Eq. (31) accelerates the convergence of Eq. (20). The value $M\omega = 0.3$ is approximately the real part of the fundamental quasinormal mode frequency of a Schwarzschild black hole [34] and dominates the emission of energy in the form of gravitational waves [12]. The source terms are largest near $r \simeq 3M$, which corresponds approximately to the location of peak of the Zerilli potential $r_{\ell=2,\,\text{peak}}^{(+)} \simeq 3.1M$ and of the light ring $r = 3M$.

The success of the Nakamura-Sasaki-Shibata transformation opens two questions. First, can we, even for a radially infalling particle, make the source term decay more rapidly? Second, can we generalize Eqs. (28) and (29) to the case in which the particle plunges with a nonzero angular momentum? In the next section we give positive answers to both questions.

B. The case of general plunging trajectories

We seek a minimal extension of Eqs. (28) and (29) for the case of a plunging particle with general angular momentum $\mathcal{L} \neq 0$. We focus only on the source term in the Zerilli equation, because the source term in the Regge-Wheeler equation already has a fast falloff:

$$S_{\ell m\omega}^{(-)} \simeq x^{-2}, \qquad x \to \infty. \qquad (33)$$

We would like to make the source term in the Zerilli equation to decay at least as rapidly as the source term for the Regge-Wheeler equation.

Our strategy is to retain Eq. (28), but generalize $Q_{\ell m\omega}$ to the form

$$Q_{\ell m\omega} = -\frac{8\pi\mu\mathcal{A}_{\ell m}}{\omega^2}\frac{f}{\Lambda r}\left[\sum_{n=0}^{N} a_n(2M/r)^{(n+1)/2}\right] \\ \times e^{i(\omega t_p - m\phi_p)}. \qquad (34)$$

Proceeding as in the previous section, we arrive at the same Eq. (31), where $S_{\ell m\omega}^{(+)}$ is now given by a more complicated formula, whose form can be found in Eq. (A1), Appendix A. We then expand Eq. (31) in a power series in r for $r \to \infty$, and collect powers in r. Next, we fix the coefficients a_n in such a way to cancel each successive power of r in this power series. This yields

$$a_0 = 1, \quad a_1 = \frac{im}{\ell(\ell+1)}\frac{\mathcal{L}}{M}, \quad a_2 = 1 - \frac{\mathcal{L}^2}{8M^2}, \qquad (35)$$

by working up to $N = 2$. Higher-order terms can be obtained by following the same procedure just outlined. We notice there is no dependence on $\mathcal{L}$ at order $N = 0$ and that we recover Eq. (29) in this case. The next correction to the radial infall case occurs at $n = 2$.

In Fig. 4 we show the original source term of the Zerilli equation $S_{\ell m\omega}^{(+)}$ and its transformed version $\tilde{S}_{\ell m\omega}^{(+),(N)}$ (for $N = 0, 1,$ and 2) for $\ell = m = 2$, $M\omega = 0.3$ and a near-critical geodesic with $\mathcal{L} = 0.9999\mathcal{L}_{\text{crit}}$. We chose this value of $\mathcal{L}$ as a "stress test" for the method, due to the large amplitude of the source term around the location of the
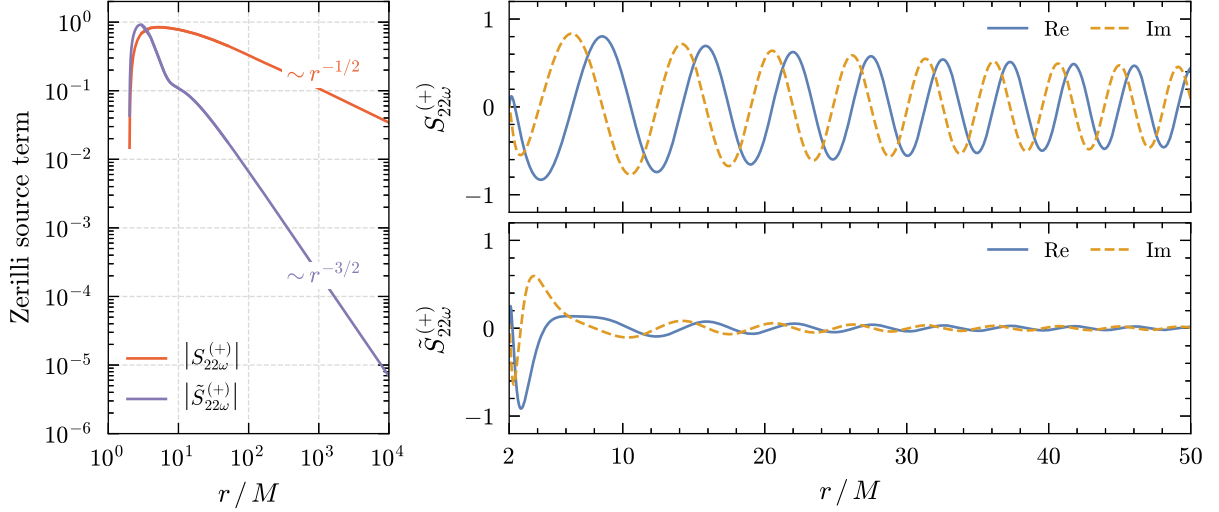
FIG. 3. The $\ell = m = 2$ source term for the Zerilli equation for a radially plunging particle starting from rest at spatial infinity, for $M\omega = 0.3$. Left panel: the absolute values of the original Zerilli source term, $S^{(+)}$, and its Nakamura-Sasaki-Shibata-transformed version, $\tilde{S}^{(+)}$. Right panels: the real ("Re") and imaginary ("Im") parts of $S^{(+)}$ (top) and $\tilde{S}^{(+)}$ (bottom). Both sources vanish at the event horizon $r = 2M$, and the faster asymptotic decay of $\tilde{S}^{(+)}$ improves the convergence of Eq. (20). The source terms are largest near $r \simeq 3M$, which corresponds approximately to the location of the peak of the Zerilli potential $r^{(+)}_{\ell=2,\,\text{peak}} \simeq 3.1M$ and of the light ring $r = 3M$.
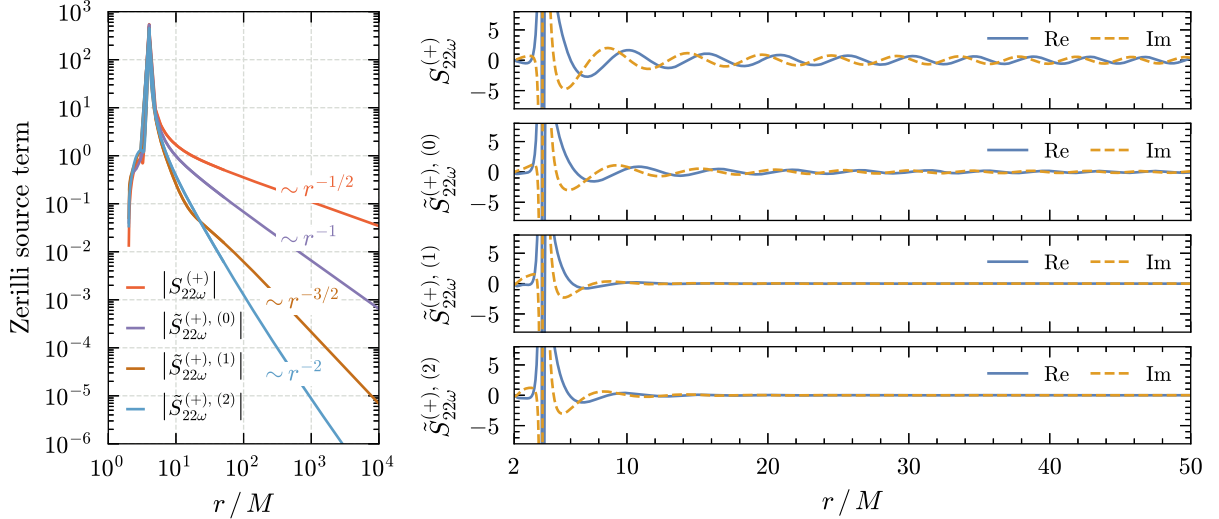

FIG. 4. The $(\ell, m) = (2, 2)$ source term for the Zerilli equation for a plunging particle with $\mathcal{L} = 0.9999\mathcal{L}_{\text{crit}}$ starting from rest at spatial infinity, for $M\omega = 0.3$. Left panel: the absolute values of the original Zerilli source term, $S^{(+)}$, and its Nakamura-Sasaki-Shibata-transformed version, $\tilde{S}^{(+),(N)}$, for $N = 0$, 1, and 2 in the expansion (34). Right panels: the real ("Re") and imaginary ("Im") parts of $S^{(+)}$ (top) and $\tilde{S}^{(+),(N)}$ (three remaining panels) for increasing values of N. The source term is largest near $r \simeq 4M$, that corresponds to the location of the marginally stable circular orbit at which the particle particle executes an increasing number of revolutions in the limit $\mathcal{L}/\mathcal{L}_{\text{crit}} \to 1$.

marginally stable circular orbit, $r = 4M$. This peak dominates over the peak at light ring $r = 3M$ present in Fig. 3. The left panel shows the absolute values of the various source terms, whereas in the right panels we show their real (solid lines) and imaginary parts (dashed lines).

We see that the original Nakamura-Sasaki-Shibata transformation ($N = 0$) results in a slower decaying source term, r^{-1}, when applied to case in which $\mathcal{L} \neq 0$, when compared

to the radial infall case, $r^{-3/2}$. This can be understood by examining the asymptotic behavior of $S^{(+)}_{\ell m\omega}$:

$$S^{(+)}_{\ell m\omega} = -\frac{4\pi\mu\mathcal{A}_{\ell m}}{\lambda M}\left[\sqrt{\frac{2M}{r}} + \frac{im}{\ell(\ell+1)}\frac{\mathcal{L}}{M}\frac{2M}{r}\right.$$
$$\left. + \left(\frac{\mathcal{L}^2}{8M^2} + \frac{3+2\lambda}{2\lambda}\right)\left(\frac{2M}{r}\right)^{3/2}\right] + \mathcal{O}(r^{-2}). \quad (36)$$

This expansion shows that the first term containing the angular momentum $\mathcal{L}$ appears at order r^{-1}, and it cannot be canceled with Eq. (29).

V. NUMERICAL METHODS AND RESULTS

In this section we describe the numerical methods we use to compute Eq. (24), and show a few applications of solving this equation using the generalized Nakamura-Sasaki-Shibata transformation (34).

A. Numerical methods

To evaluate our main quantity of interest, namely the amplitude $C_{\ell m\omega}^{(\pm),\,\mathrm{out}}$ we proceed as follows:

(1) Choose a value of ℓ, $|m| \leq \ell$, and $M\omega$.
(2) Choose a value of the angular momentum $\mathcal{L}$, and solve the geodesic equations (5), to obtain $t_p(r)$ and $\phi_p(r)$. We use initial conditions $t_p(r_{\min}) = 0$ and $\phi_p(r_{\min}) = 0$, and integrate from $r_{\min} = 2(1 + 10^{-4})M$ up to $r_{\max} = 500/\omega$.
(3) If $\ell + m$ is even, integrate the homogeneous Zerilli equation. If $\ell + m$ is odd, integrate the homogeneous Regge-Wheeler equation; see Eqs. (11) and (14).
(4) Integrate the equation from the previous step with "in" boundary conditions, from $r_{\min} = 2(1 + 10^{-4})M$ to $r = r_{\max}$. From $X_{\ell m\omega}^{(\pm)}$ and $dX_{\ell m\omega}^{(\pm)}/dr$ at $r_{\max}$ calculate $A_{\ell m\omega}^{(\pm),\,\mathrm{in,out}}$. See Appendix C.
(5) Calculate the Wronskian (23) and the source $S_{\ell m\omega}^{(\pm)}$ to evaluate the integral in Eq. (24).
(6) Repeat steps 1 through 5, scanning the range $M\omega \in [5 \times 10^{-3}, 1.5]$ in steps of size $\Delta(M\omega) = 5 \times 10^{-3}$, for $\ell = 2$ to 6, covering all $|m| \leq \ell$ in between.

Our code is written in *Mathematica*. In step 3, we validated our integration of the homogeneous equations (14) by comparison against the integrators available in the Black Hole Perturbation Toolkit [35]. Recursion relations for the near-horizon and far-field expansions of the Regge-Wheeler and Zerilli functions are summarized in Appendix B. In step 5, we calculate the Wronskian as explained in Appendix C, and it is useful to rewrite Eq. (24) as a differential equation [36,37]:

$$\frac{dC_{\ell m\omega}^{(\pm),\,\mathrm{out}}}{dr} = \frac{1}{W_{\ell m\omega}^{(\pm)}} f^{-1} X_{\ell m\omega}^{(\pm),\,\mathrm{in}} S_{\ell m\omega}^{(\pm)}. \qquad (37)$$

We integrate Eq. (37), with initial condition $C_{\ell m\omega}^{(\pm),\,\mathrm{out}}(r_{\min}) = 0$ up to $r_{\max}$, using the Regge-Wheeler source (A6) or the Nakamura-Sasaki-Shibata-transformed Zerilli source (31), depending on whether $\ell + m$ is odd or even, respectively. In the context of Eq. (37), the new Zerilli source term reduces the value of $r_{\max}$ at which $dC_{\ell m\omega}^{(\pm),\,\mathrm{out}}/dr$ becomes zero to the desired accuracy. We

decided here only, with respect to the rest this work, to integrate the geodesic equations from near the horizon outwards. In particular, when integrating from spatial infinity, t_p acquires a large value around $r \approx 2M$. This causes the factor $\exp(i\omega t_p)$, which appears in the source, to become highly oscillatory, and thus sensitive to our choice of $r_{\min}$ and ω. Consequently, the phase (but not the amplitude) of the $C_{\ell m\omega}^{(\pm),\,\mathrm{out}}$ failed to converge in our numerical calculations. We solved this issue by fixing the initial conditions at the horizon instead of spatial infinity. At last, we performed steps 1 to 6 for the range of angular momentum values $\mathcal{L} = \{0, 0.25, 0.5, 0.75, 0.9, 0.99, 0.999, 0.9999\}\mathcal{L}_{\mathrm{crit}}$.

B. Energy spectrum

We first consider the energy spectrum for the particle in the near-critical limit $\mathcal{L} \approx \mathcal{L}_{\mathrm{crit}}$. To our knowledge, this situation was studied only in the frequency domain using the Sasaki-Nakamura equation [29] or using the Zerilli-Moncrief [26] and Cunningham-Price-Moncrief [25] master functions in Ref. [38]. To validate our calculations, we focus on two cases, $\mathcal{L}/\mathcal{L}_{\mathrm{crit}} = 0.9$ and 0.9999, which were examined in detail by Berti *et al.* [29].

In Fig. 5, we show the energy spectrum (21) for $\mathcal{L} = 0.9\mathcal{L}_{\mathrm{crit}}$ (left panels) and $\mathcal{L} = 0.9999\mathcal{L}_{\mathrm{crit}}$ (right panels). The top panels show the spectral energy for multipoles $\ell = m$ ranging from 2 to 6 (different line colors) and their sum (dashed line). The bottom panels show the quadrupole mode $\ell = 2$ and all azimuthal contributions $|m| \leq 2$ (different line styles.) Our results are in excellent agreement with those of Ref. [29]; cf. Figs. 10 and 11 therein.

For $\mathcal{L} = 0.9\mathcal{L}_{\mathrm{crit}}$, the energy radiated in each multipole $\ell = m$ has a single maximum. The location $M\omega$ of these peaks coincide approximately with the real part of the fundamental ($n = 0$) quasinormal mode frequency of a Schwarzschild black hole $M\omega_{\ell m0}$, as first observed by Detweiler and Szedenits [12]. For reference, these values are $\mathrm{Re}[M\omega_{\ell m0}] \simeq \{0.373, 0.599, 0.809, 1.012, 1.212\}$, for $\ell \in \{2, 6\}$ [39–41]. (Due to the spherical symmetry of the Schwarzschild solution, all quasinormal modes with $|m| \leq \ell$, at fixed $\ell \geq 2$, are degenerate.)

In the near-critical limit $\mathcal{L} = 0.9999\mathcal{L}_{\mathrm{crit}}$, the spectral energy distribution has a peak at $M\omega < \mathrm{Re}[M\omega_{\ell m0}]$. This peak corresponds to m times the particle's orbital frequency $M\Omega_{\mathrm{orb}} = 1/8$ at the marginally stable circular orbit at $r = 4M$ (cf. Fig. 2), that is

$$M\omega = mM\Omega_{\mathrm{orb}} = m/8. \qquad (38)$$

Therefore, the energy emitted at these frequencies is dominated by the particle's geodesic motion. This is not surprising given that we saw that the maximum amplitude of the source term of the Zerilli equation is located at $r \simeq 4M$, as we discussed in Fig. 4. For moderate values of
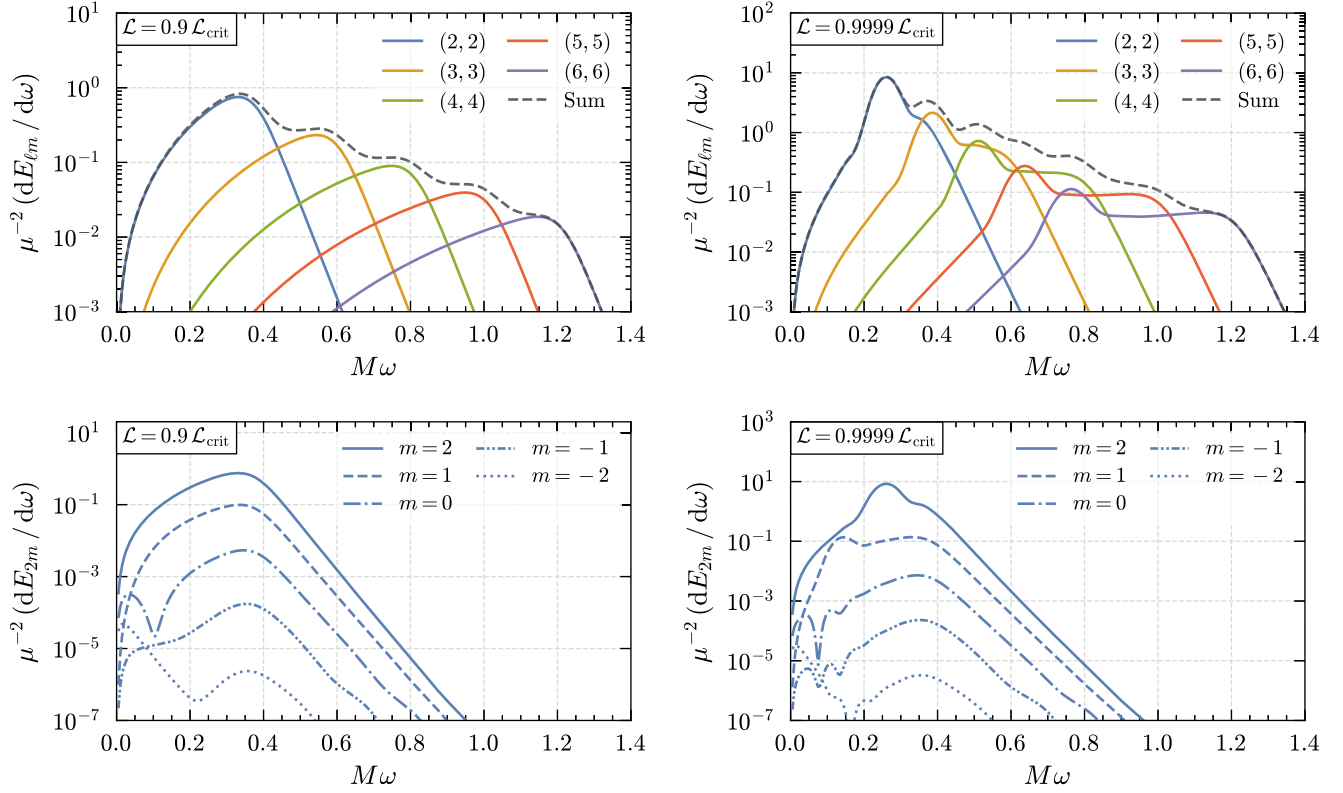
FIG. 5.　The energy spectra for a particle plunging with angular momentum $\mathcal{L} = 0.9\mathcal{L}_{\mathrm{crit}}$ (left panels) and $\mathcal{L} = 0.9999\mathcal{L}_{\mathrm{crit}}$ (right panels) into a Schwarzschild black hole. Top panels: the energy spectra from the multipoles $\ell = m$ from 2 to 6, (colored lines), and their sum (dashed line). Bottom panels: the energy spectra for the quadrupole perturbation $\ell = 2$ and all $|m| \leq 2$ in between. Note the different ranges in the ordinates across the panels. Our results agree with Ref. [29], which solved the Sasaki-Nakamura equation instead.

ℓ, the contributions to the energy driven by the particle's orbital motion and the quasinormal mode excitation overlap, while as $\ell \gg 1$ their contributions separate sufficiently to result in two peaks in the energy spectra; see the $\ell = m = 5$ and 6 in Fig. 5. For $\ell = m = 5$ the peaks are located at $M\omega \simeq 0.637$ and 0.919, while for $\ell = m = 6$ they are found at $M\omega \simeq 0.763$ and 1.125. We can estimate this separation as follows. First, we use the geometrical-optics (eikonal) limit [42–44], to approximate the real part of the quasinormal mode frequency as

$$\mathrm{Re}[M\omega_{\mathrm{eik}}] \simeq \ell\Omega_{\mathrm{LR}} = \ell/(3\sqrt{3}), \tag{39}$$

where $M\Omega_{\mathrm{LR}} = 1/(3\sqrt{3})$ is the orbital frequency of a null geodesic at the light ring. Equation (39) can also be obtained from the $\ell \gg 1$ limit of a Wentzel-Kramers-Brillouin approximation to the calculation of black-hole quasinormal modes [45,46]. We can then estimate the separation between the "quasinormal-mode" and "geodesic" peaks by taking the difference of Eqs. (38) and (39):

$$(\Delta M\omega)_{\mathrm{peak}} \simeq \frac{1}{3\sqrt{3}}\left(\ell - \frac{3\sqrt{3}}{8}m\right), \tag{40}$$

which is valid for $\ell \gg 1$, $\mathcal{L}/\mathcal{L}_{\mathrm{crit}} \simeq 1$, and $\mathcal{E} = 1$. For $\ell = m = 6$, we find $(\Delta M\omega)_{\mathrm{peak}} \simeq 0.404$, in fair agreement with the numerical result $\simeq 0.362$, obtained from the difference between the two peak locations.

Although not studied here, it is interesting to analyze the ultrarelativistic limit, in which the particle plunges with an energy $\mathcal{E} \to \infty$. In this limit, the "geodesic" peak moves rightwards, eventually overlapping with the "quasinormal-mode" peak; see Ref. [29], Fig. 10. This occurs because as $\mathcal{E} \to \infty$, the particle's marginally stable circular orbit coincides with the light ring, hence $\Omega_{\mathrm{orb}} \simeq \Omega_{\mathrm{LR}}$ [31]. In this limit, we then have

$$(\Delta M\omega)_{\mathrm{peak}} = (\ell - m)(3\sqrt{3}), \tag{41}$$

which is valid for $\ell \gg 1$, $\mathcal{L}/\mathcal{L}_{\mathrm{crit}} \simeq 1$, and $\mathcal{E} \to \infty$. The peak separation vanishes when $\ell = m$, reproducing the results of Ref. [29].

C. Total energy

From the energy spectrum, we can compute the total energy ΔE emitted in form of gravitational waves by

integrating the spectrum density and summing the contributions from all multipoles:

$$\Delta E = \sum_{\ell=2}^{\infty} \Delta E_\ell = \sum_{\ell=2}^{\infty} \sum_{m=-\ell}^{\ell} \int_0^{+\infty} d\omega \frac{dE_{\ell m}}{d\omega}. \quad (42)$$

To understand the relative contribution due to perturbations of each parity, we also define $\Delta E^{(\pm)}$, where the subscript $(+)$ means we add only the contributions to the energy coming from multipoles for which $\ell + m$ is even and $(-)$ when $\ell + m$ is odd.

For particles that plunge from infinity initially from rest, Oohara and Nakamura [20], based on an earlier observation by Davis *et al.* [6] for the case $\mathcal{L} = 0$, proposed the empirical relation

$$(M/\mu^2)\Delta E_\ell = a \exp(-b\ell), \quad (43)$$

between energy and multipole ℓ. We fit Eq. (43) to the outcome of computing ΔE_ℓ, truncating the ℓ sum at $\ell_{\max} = 6$. Table I shows the fitting coefficients and the total energy emitted, including the individual polar and axial contributions. The results for the total energy agree with those of Ref. [29], Table II, with less than 1% difference, when comparison is possible. As observed by Oohara and Nakamura, the value of a increases while that of b decreases as $\mathcal{L}$ approaches $\mathcal{L}_{\text{crit}}$. In other words, the fraction of the total energy radiated contained in each ℓ pole tends to "even out" as $\mathcal{L}$ increases.

Figure 6 illustrates these observations. For example, we see in the leftmost panel that ΔE_2 varies from being about four orders of magnitude larger than ΔE_6, to being some more than ten times larger as $\mathcal{L}$ approaches criticality. The individual contributions of the polar and axial perturbations to the energy are shown in the middle and rightmost panels, respectively. We see that the energy emitted through the "axial radiative channel" is always subdominant relative to the polar one, even for near-critical values of $\mathcal{L}$; the extreme case is, of course, when $\mathcal{L} = 0$ where $\Delta E^{(-)}$ vanishes.

Interestingly, the axial and polar contributions to the total energy ΔE are nonmonotonic with respect to the angular momentum. In Fig. 7, we show the ratio $\Delta E^{(\pm)}/\Delta E$ as a function of the logarithm of $1 - \mathcal{L}/\mathcal{L}_{\text{crit}}$. As we increase the particle's angular momentum (i.e., moving right to left along the abscissa), we see that $\Delta E^{(-)}/\Delta E$ has a local maximum at $\mathcal{L} \approx 0.75\mathcal{L}_{\text{crit}}$, yet with only approximately 14% of the total energy budget. We interpret this result as follows. When $\mathcal{L} = 0$, by symmetry, all energy must be radiated through the polar channel. As we increase $\mathcal{L}$, axial perturbations become increasingly excited, and a nonzero (albeit small) percentage of the energy is emitted through them. As $\mathcal{L}$ approaches $\mathcal{L}_{\text{crit}}$, the particle orbits the black hole an increasing number of times around the circular orbit $r = 4M$. Hence, again by symmetry, we expect the total energy fraction emitted through the polar channel to increase, and it happens to the extent of thereby decreasing the fraction emitted through the axial channel.

D. Time-domain waveforms

We also computed the time-domain Regge-Wheeler and Zerilli mode functions using Eq. (22). In Fig. 8, we show the dominant modes for the Regge-Wheeler and Zerilli functions, $(\ell, m) = (2, 1)$ and $(2,2)$, respectively, as a function of the retarded time $(t - x)/M$. The top panel corresponds to a particle that plunges with $\mathcal{L} = 0.9\mathcal{L}_{\text{crit}}$, while the bottom panel to $\mathcal{L} = 0.9999\mathcal{L}_{\text{crit}}$. In the former case, we see that the waveform has the characteristic "precursor," "sharp burst," and "ringing tail" phases, as first observed for radial infalling particles by Davis *et al.* [8] and for wave scattering by Vishveshwara [47]. As $\mathcal{L} \to \mathcal{L}_{\text{crit}}$, the large values of $\mathcal{L}$ cause the Zerilli (but not the Regge-Wheeler) function to have an intermediate quasimonochromatic phase, related to the particle's sweep around $r = 4M$. This behavior is qualitatively the same as that seen in Refs. [48,49] for test particles plunging from the innermost stable circular orbit $r = 6M$. We see that the amplitude of the Regge-Wheeler function is always smaller than Zerilli's, even in the nearest-critical angular-momentum values studied by us.

TABLE I. Coefficients a and b in the Oohara-Nakamura relation (43) and the total energy $(\mu^2/M)\Delta E$ for different values of angular momentum $\mathcal{L}$. The superscripts refer to polar $(+)$ and axial-parity $(-)$ perturbations.

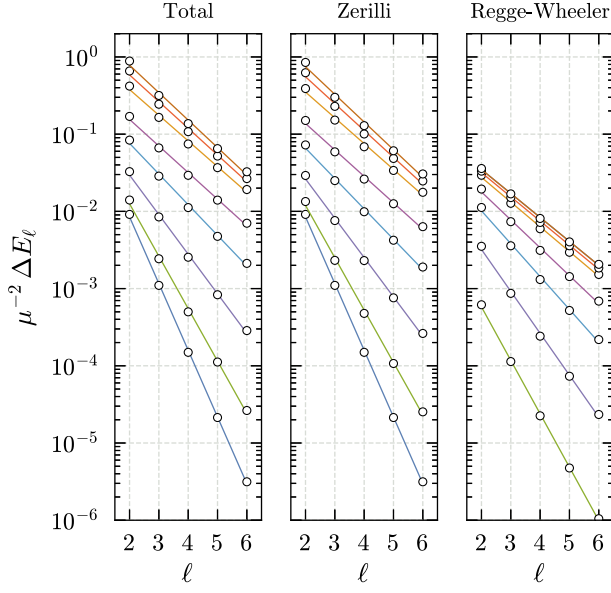| $\mathcal{L}/\mathcal{L}_{\text{crit}}$	a	b	$a^{(+)}$	$b^{(+)}$	$a^{(-)}$	$a^{(-)}$	ΔE $\times 10^{-2}$	$\Delta E^{(+)}$ $\times 10^{-2}$	$\Delta E^{(-)}$ $\times 10^{-4}$
0.0000	0.45	1.99	0.45	1.99	$\cdots$	$\cdots$	1.04	1.04	$\cdots$
0.2500	0.29	1.56	0.27	1.56	0.01	1.59	1.71	1.63	7.59
0.5000	0.31	1.18	0.27	1.17	0.04	1.25	4.48	4.01	47.4
0.7500	0.47	0.91	0.40	0.91	0.07	0.98	13.0	11.4	169
0.9000	0.76	0.79	0.66	0.79	0.09	0.83	28.7	25.4	321
0.9900	1.75	0.77	1.63	0.77	0.12	0.74	71.5	66.2	525
0.9990	2.88	0.80	2.75	0.80	0.13	0.72	109	103	609
0.9999	4.02	0.82	3.89	0.82	0.15	0.71	144	137	669

FIG. 6. Energy radiated to infinity in the plunge process. From left to right, the panels show the total energy radiated, only through the parity even ("Zerilli") perturbations, and only through the parity odd ("Regge-Wheeler") perturbations. The markers correspond to Eq. (42), whereas the straight lines corresponds to the fit (43) suggested by Oohara and Nakamura 20]]. The lines starting from the bottom correspond to $\mathcal{L} = 0$ and increase to $\mathcal{L} = 0.9999\mathcal{L}_{\text{crit}}$ as one moves upwards. The energy emitted in the dominant quadrupole mode in the axial-parity radiative channel is always smaller than that emitted through the polar one, at fixed $\mathcal{L}$. When $\mathcal{L} = 0$, there is no energy radiated in the axial-parity channel.
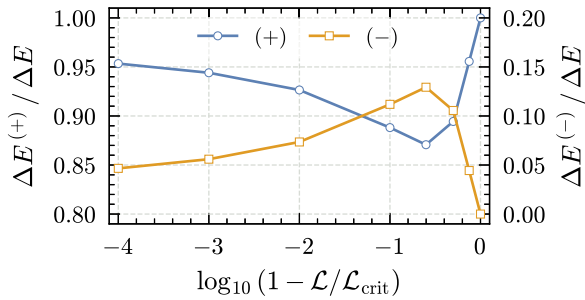

FIG. 7. Fraction of the total energy radiated by the polar and axial perturbations in the plunge process. We show both the polar [(+), left ordinate] and axial [(−), right ordinate] total energies as functions of the particle's angular momentum. The fraction of the total energy radiated via each radiative channel is nonmonotonic in $\mathcal{L}$, with the axial channel having a peak at $\mathcal{L}/\mathcal{L}_{\text{crit}} \approx 0.75$. The polar contribution is at least $\approx 85\%$ of the total energy budget for all values of $\mathcal{L}$ considered.
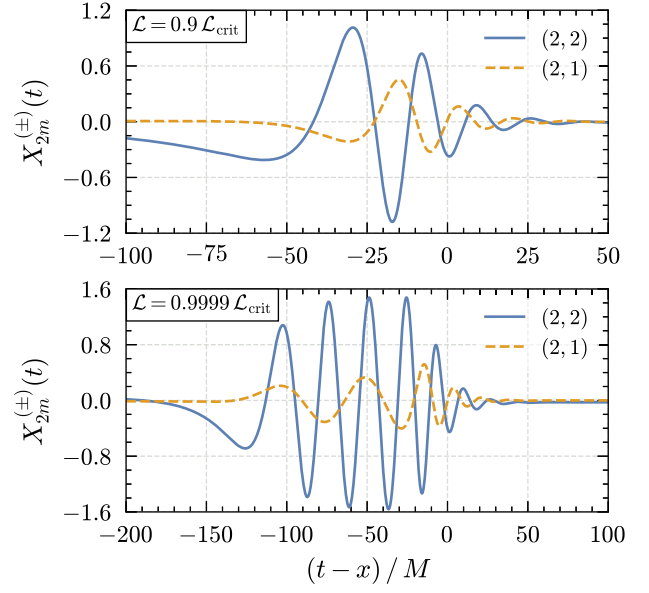

FIG. 8. Time-domain Zerilli (solid lines) and Regge-Wheeler (dashed lines) mode functions excited by a test particle plunging with $\mathcal{L} = 0.9\mathcal{L}_{\text{crit}}$ (top panel) and $\mathcal{L} = 0.9999\mathcal{L}_{\text{crit}}$ (bottom panel) into a Schwarzschild black hole. We focus on the dominant quadrupole multipole, associated with the perturbations of each parity: $m = 2$ and $m = 1$ for the Zerilli and Regge-Wheeler modes, respectively. The former is always larger in amplitude than the latter.

In Fig. 9, we take a closer look on the waveforms in the limit $\mathcal{L} \to \mathcal{L}_{\text{crit}}$, for the same multipole moments. In this limit, the waveforms become increasingly similar around their peak amplitudes, $t − x \simeq −40M$, although differences are clearly visible at the "precursor" phase. Similar results hold for the other multipoles we examined. This result suggests that a quasiuniversal description of the plunge from the marginally stable circular orbit $r = 4M$ exists. Such a treatment for particle's plunging from the innermost stable circular orbit exists [50].

VI. THE SEMIRELATIVISTIC APPROXIMATION

A complementary way of studying the gravitational wave emission by an infalling particle is via the so-called semirelativistic approximation [30] (often used in the "kludge" approximation [51–53]). In this approach the particle is assumed to move along a fully relativistic geodesic trajectory of the black-hole spacetime while the gravitational wave emission itself is treated approximately, using the weak-gravity quadrupole formula.

Despite its inherent inconsistency, the semirelativistic approximation is known to perform surprisingly well, when compared against more rigorous results obtained from black-hole perturbation theory. The price one has to pay for the conceptual and technical simplicity of this approach
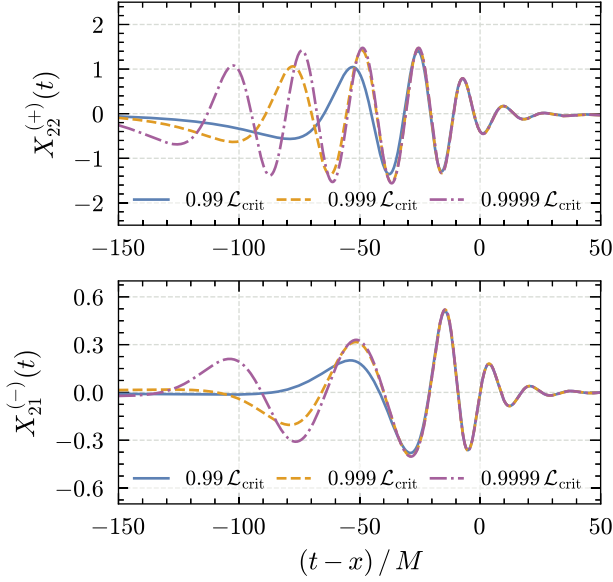
FIG. 9. Time-domain Zerilli (top panel) and Regge-Wheeler (bottom panel) mode functions excited by a test particle plunging with $\mathcal{L} = 0.99\mathcal{L}_{\text{crit}}$ (solid lines), $\mathcal{L} = 0.999\mathcal{L}_{\text{crit}}$ (dashed lines), and $\mathcal{L} = 0.9999\mathcal{L}_{\text{crit}}$ (dot-dashed lines) into a Schwarzschild black hole. As in Fig. 8, we consider the dominant quadrupolar Zerilli and Regge-Wheeler modes. In the limit $\mathcal{L} \to \mathcal{L}_{\text{crit}}$, the solutions become quasiuniversal around and after $t - x \gtrsim -40M$.

is that its accuracy deteriorates as soon as the particle's trajectory enters the near horizon, strong field regime where radiation backscattering by the spacetime curvature becomes an important factor. Unfortunately, this condition is clearly met by a plunging particle so we expect the semirelativistic method to provide accurate results only for the early time portion of the trajectory (i.e., the low frequency part of the gravitational wave spectrum.) Nevertheless, the less accurate $\omega M \gtrsim 1$ part of the spectrum is of some interest in its own right as it allows us to understand (and separate) the effects due to the particle's motion and due to backscattering.

The quadrupole-order gravitational-wave formalism underpinning the semi-relativistic approximation can be found in many general relativity textbooks; here we follow and expand the analysis of Ref. [54], Sec. IV.3.1, for radially infalling particles.

We start by recalling that the appropriately averaged gravitational-wave luminosity is given by

$$L = \frac{1}{5}\left\langle \dddot{M}_{ij}\dddot{M}^{ij} - \frac{1}{3}\dddot{M}^2 \right\rangle, \tag{44}$$

where the (mass) quadrupole moment M_{ij} is defined as

$$M^{ij}(t) = \int \mathrm{d}^3 x \rho(t, \boldsymbol{x}) x^i x^j, \tag{45}$$

for a mass density $\rho(t, \boldsymbol{x})$, and with trace $M = M^i{}_i$, which is distinguishable from the black hole's mass M from the context. The total energy emitted in gravitational waves is given by the integral

$$\Delta E = \int_{-\infty}^{t_{\max}} \mathrm{d}t L(t), \tag{46}$$

where the luminosity is to be evaluated without any averaging (also, we can set $t_{\max} = \infty$ at the particle's horizon crossing time). The same quantity can be evaluated in the frequency domain

$$\Delta E = \int_0^{+\infty} \mathrm{d}\omega \frac{\mathrm{d}E}{\mathrm{d}\omega}, \tag{47}$$

where $\mathrm{d}E/\mathrm{d}\omega$ is the spectral energy distribution.

For a point particle moving along a trajectory $\boldsymbol{x}_p(t)$ we have $\rho(t, \boldsymbol{x}) = \mu\delta^{(3)}[\boldsymbol{x} - \boldsymbol{x}_p(t)]$, and we find

$$M^{ij}(t) = \mu x_p^i(t)x_p^j(t). \tag{48}$$

As in Sec. II, the geodesics under consideration can be taken to lie in the equatorial x-y plane and the Cartesian coordinates can be related to the Schwarzschild-Droste coordinates (1) through Eq. (6). In this setup, the only nonvanishing components of the quadrupole moment (45) are M_{11}, M_{22}, M_{12}, and the trace is $M = M_{11} + M_{12}$. Then, a short calculation leads to

$$
\begin{aligned}
\Delta E &= \frac{2}{15}\int_{-\infty}^{+\infty} \mathrm{d}t[\dddot{M}_{11}^2 + \dddot{M}_{22}^2 - \dddot{M}_{11}\dddot{M}_{22} + 3\dddot{M}_{12}^2], \\
&= \frac{2}{15\pi}\int_0^{+\infty} \mathrm{d}\omega\omega^6[|\tilde{M}_{11}|^2 + |\tilde{M}_{22}|^2 + 3|\tilde{M}_{12}|^2 \\
&\quad - \mathrm{Re}[\tilde{M}_{11}\tilde{M}_{22}^*]],
\end{aligned}
\tag{49}
$$

where the Fourier transform of M_{ij} is defined as[3]

$$\tilde{M}_{ij}(\omega) = \int_{-\infty}^{+\infty} \mathrm{d}t e^{i\omega t} M_{ij}(t). \tag{50}$$

The fact that M_{ij} is real implies the useful property

$$\tilde{M}_{ij}^*(\omega) = \tilde{M}_{ij}(-\omega). \tag{51}$$

As discussed in Ref. [54], the integral (50) is divergent at $t \to -\infty$, since $x_p \to +\infty$. Therefore, some regularization procedure is required. This is achieved by working with the Fourier transform $\tilde{\tilde{M}}_{ij}$, which is well behaved at spatial infinity. In fact, this procedure is equivalent to the regularization of $\tilde{M}_{ij}(\omega)$ via integrations by parts, where the

---

[3]For clarity, we adopt a slightly different notation for frequency-domain quantities in this section, mirroring Ref. [54].

produced divergent boundary terms are discarded (see, e.g., Detweiler and Szedenits [12] for a similar regularization of the solution of the Teukolsky equation sourced by a plunging particle). The outcome of this exercise is the regularized quadrupole moment

$$\tilde{M}_{ij}^{\text{reg}} = -\tilde{\ddot{M}}_{ij}/\omega^2, \tag{52}$$

and from Eq. (49) we read off the regularized formula:

$$\frac{\mathrm{d}E}{\mathrm{d}\omega} = \frac{2\omega^2}{15\pi} \big[|\tilde{\ddot{M}}_{11}|^2 + |\tilde{\ddot{M}}_{22}|^2 + 3|\tilde{\ddot{M}}_{12}|^2 - \mathrm{Re}[\tilde{\ddot{M}}_{11}\tilde{\ddot{M}}_{22}^*]\big]. \tag{53}$$

For the actual numerical evaluation of $\tilde{\ddot{M}}_{ij}$ (and the subsequent one of $\mathrm{d}E/\mathrm{d}\omega$), it is advantageous to convert the time integral into a radial integral using the geodesic equations (2), leading to

$$\tilde{\ddot{M}}_{ij} = \int_{2M}^{r_{\max}} \frac{\mathrm{d}r}{f} \left[\frac{2M}{r} + f\frac{\mathcal{L}^2}{r^2}\right]^{-\frac{1}{2}} \ddot{M}_{ij} e^{i\omega t_p(r)}. \tag{54}$$

For the problem at hand, the individual $\ddot{M}_{ij}$ components required for the calculation of Eq. (52) are

$$\ddot{M}_{11} = 2\mu(x_p\ddot{x}_p + \dot{x}_p^2), \tag{55a}$$

$$\ddot{M}_{22} = 2\mu(y_p\ddot{y}_p + \dot{y}_p^2), \tag{55b}$$

$$\ddot{M}_{12} = \mu(2\dot{x}_p\dot{y}_p + x_p\ddot{y}_p + y_p\ddot{x}_p). \tag{55c}$$

With the help of Eq. (2) both the accelerations $\ddot{x}_p$, $\ddot{y}_p$ and the velocities $\dot{x}_p$, $\dot{y}_p$ can be rewritten solely as functions of r, $\phi_p(r)$ and the orbital constant $\mathcal{L}$. At the same time $t_p(r)$ explicitly appears in the exponential term. Both $\phi_p(r)$ and $t_p(r)$ are obtained numerically as in Sec. II. We chose trajectories with $\phi_p(0) = 0$ at some initial radius $r_{\max} = r(0)$. The same radius serves as the "infinity" upper limit in the $\tilde{\ddot{M}}_{ij}$ integral. The initial time $t = 0$ can be chosen arbitrarily because the addition of a constant in $t_p(r)$ does not affect the numerical value of Eq. (54).

For any value $\mathcal{L} < \mathcal{L}_{\text{crit}}$, the integral in the $\tilde{\ddot{M}}_{11}$ component is the slowest converging one at large r (the absolute value of the integrand decays as $\sim r^{-1/2}$). In order to improve the convergence of this component and reduce the associated numerical error we employ a procedure similar to that in Sec. IV B, namely, we subtract the slowly decaying part prior to the numerical integration and then add back the (analytically obtained) asymptotic contribution from that part.

The semirelativistic energy spectrum, calculated from Eqs. (53) and (54), is shown in Fig. 10 and has a characteristic single-hump profile. When comparing against the full black-hole perturbation theory result for $\ell = m = 2$ shown in Fig. 5, we notice a moderate
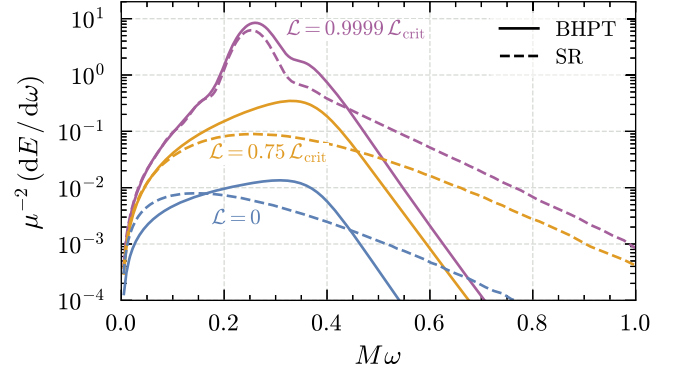

FIG. 10. The energy spectra for a particle plunging with angular momentum $\mathcal{L} = 0$, $\mathcal{L} = 0.75\mathcal{L}_{\text{crit}}$, and $\mathcal{L} = 0.9999\mathcal{L}_{\text{crit}}$ into a Schwarzschild black hole in the semirelativistic approximation ("SR," dashed lines) and black-hole perturbation theory, for $\ell = m = 2$ ("BHPT," solid lines). Both calculations agree at low frequencies $M\omega \ll 1$, where the radiation is due to the particle's quasi-Newtonian motion. For $\mathcal{L} = 0$ and $\mathcal{L} = 0.75\mathcal{L}_{\text{crit}}$, the kludge calculation underestimates the location of the spectrum's peak, which is related to the hole's fundamental quasinormal mode frequency [12]. As $\mathcal{L} \to \mathcal{L}_{\text{crit}}$, the peak of the spectrum is dominated by the particle's orbit around $r = 4M$, and the two calculations agree qualitatively with each other up to $M\omega \lesssim 0.25$. The semirelativistic approximation predicts a slowly decaying tail for the spectrum.

disagreement in the location of the emission peak. This is not surprising because the exact location of this peak depends on the properties of the BH potential near $3M$; as pointed out earlier, this information is missing altogether in the semirelativistic approximation. As expected, the two spectra are in good agreement in the low frequency, $\omega M \ll 1$, end of the spectrum which is the part that corresponds to quasi-Newtonian motion, that is, when the particle is still moving far away from the black-hole horizon. Interestingly, the agreement improves to some degree as we approach the critical value $\mathcal{L}_{\text{crit}}$ for scattering. In this case, the particle spends a large amount of time orbiting around $r = 4M$ and the bulk of gravitational-wave emission is generated there, as we have discussed in Sec. V.

The opposite high-frequency end of the spectrum, $\omega M \gg 1$, has also some interest of its own. In the fully relativistic calculation, this part of the spectrum appears to be independent of the angular momentum $\mathcal{L}$ and the modal numbers ℓ and m. We can approximate the high-frequency "tail" of $\mathrm{d}E_{\ell m}/\mathrm{d}\omega$ in the special case of radial infall, taking into account that this part of the spectrum corresponds to the near-horizon region of integration in Eq. (24). Under these circumstances we can recast the integrand into a single exponential, and expand the exponent up to linear order in $r/(2M) - 1$. The integral can then be computed analytically, and it is found to be dominated by the lower limit of integration. Moreover, in the same high-frequency limit the Wronskian can be approximated as $W_{\ell m\omega} \simeq 2i\omega$. These manipulations lead to a scaling

$$\frac{\mathrm{d}E}{\mathrm{d}\omega} \propto \frac{e^{-8\pi M\omega}}{M\omega} \quad \text{(perturbation theory)}. \qquad (56)$$

The same procedure applied to the semirelativistic spectrum leads to a slower decaying tail

$$\frac{\mathrm{d}E}{\mathrm{d}\omega} \propto \frac{e^{-4\pi M\omega}}{M\omega} \text{(semirelativistic)}. \qquad (57)$$

The difference can be traced back to the additional highly oscillatory function $X_{\ell m\omega}^{(\pm),\,\text{in}} \simeq \exp(i\omega x)$ in the full black-hole perturbation theory expression, which suppresses the integral at large ω. This analysis thus explains the difference in the high-frequency tails shown in Fig. 10.

VII. CONCLUSIONS

We reviewed, and generalized, a transformation by Nakamura *et al.* [28] that makes the source term of the Zerilli function to have a faster falloff at spatial infinity, thereby improving the numerical convergence of the convolution integral that arises in the calculation of gravitational radiation by particles in unbound geodesic motion in the Schwarzschild spacetime.

As an application, we studied the gravitational radiation produced by test particles that plunge from rest and with angular momentum $\mathcal{L}$ from spatial infinity into a Schwarzschild black hole. In particular, we focused on the limit in which $\mathcal{L}$ approximates from below the critical value $\mathcal{L}_{\text{crit}}$ for scattering. To our knowledge, this is the first time this calculation was done using the original Regge-Wheeler and Zerilli master functions. Our results are in agreement with the work by Berti *et al.* [29] that used the Sasaki-Nakamura equation. We studied in detail the relative contributions to the energy radiated in gravitational waves due to perturbations of polar and axial parity. We found that the former always dominates. We also observed an quasiuniversal late-time behavior of the waveforms in limit in which $\mathcal{L}$ approaches the critical value for scattering, $4M$.

The main merit of the Nakamura-Sasaki-Shibata transformation is that it only requires minimal modifications to the source term of the Zerilli function [cf. Eqs. (29) and (31)]. The new source term can be easily computed analytically with any symbolic algebra software. In contrast, the Sasaki-Nakamura formalism requires the numerical integration of an auxiliary second-order differential equation for the calculation of the source term [16–18]. However, an advantage of the Sasaki-Nakamura formalism is that it applies to the Kerr spacetime, while the method presented here is not. Our work is alternative to that of Hopper [38] that addresses the sources of the Zerilli-Moncrief and Cunningham-Price-Moncrief master functions.

We complemented our calculations in black-hole perturbation theory, with an analysis of the same plunging-particle problem in the semirelativistic approximation.

We found that the two energy spectra agree best with in the limit $\mathcal{L} \to \mathcal{L}_{\text{crit}}$, when the energy is dominated by the particle's motion around the marginally stable circular orbit. We also studied the high-frequency limit of the spectrum, expanding upon the discussion in Ref. [54].

The method presented here can be used in other problems involving unbound motion in the Schwarzschild spacetime, including ultrarelativistic plunges [10,55], scattering [27], or in the spacetime of relativistic stars [56–59] using the Regge-Wheeler-Zerilli formalism.

APPENDIX A: THE SOURCES OF THE REGGE-WHEELER AND ZERILLI EQUATIONS

In this appendix we present the sources for the Regge-Wheeler and Zerilli equations (7), quoting from the formulas presented in Refs. [32,33]; the original derivation is due Zerilli [5].

The source $S_{\ell m\omega}^{(+)}$, which excites the perturbations of polar parity, is given by

$$
\begin{aligned}
S_{\ell m\omega}^{(+)} = {} & -if\frac{\mathrm{d}}{\mathrm{d}r}\left[\frac{f^2}{\Lambda}\left(\frac{ir}{f}\tilde{C}_{1\ell m\omega} + \tilde{C}_{2\ell m\omega}\right)\right] \\
& + i\frac{f^2}{r\Lambda^2}\left[i\frac{\lambda r^2 - 3\lambda Mr - 3M^2}{rf}\tilde{C}_{1\ell m\omega}\right. \\
& \left. + \frac{\lambda(\lambda+1)r^2 + 3\lambda Mr + 6M^2}{r^2}\tilde{C}_{2\ell m\omega}\right], \qquad (A1)
\end{aligned}
$$

where[4]

---

[4]We note that in the equation for $\tilde{B}_{\ell m\omega}$, the term proportional to $A_{\ell m\omega}^{(1)}$ in Eq. (A42) of Ref. [32] has a typo, which is corrected in Eq. (4.12) of Ref. [33].

$$\tilde{B}_{\ell m\omega} = \frac{8\pi r^2 f}{\Lambda}\left[A_{\ell m\omega} + \frac{1}{\sqrt{\ell(\ell+1)/2}}B_{\ell m\omega}\right]$$
$$- 4\pi \frac{\sqrt{2}}{\Lambda}\frac{M}{\omega}A^{(1)}_{\ell m\omega}, \tag{A2}$$

$$\tilde{C}_{1\ell m\omega} = \frac{8\pi}{\sqrt{2}\omega}A^{(1)}_{\ell m\omega} + \frac{1}{r}\tilde{B}_{\ell m\omega} - 16\pi r\left[\frac{1}{2}\frac{(\ell+2)!}{(\ell-2)!}\right]^{-\frac{1}{2}}F_{\ell m\omega}, \tag{A3}$$

$$\tilde{C}_{2\ell m\omega} = \frac{8\pi i}{\omega\sqrt{\ell(\ell+1)/2}}\frac{r}{f}B^{(0)}_{\ell m\omega} - \frac{i}{f}\tilde{B}_{\ell m\omega}$$
$$+ \frac{16\pi i r^2}{f}\left[\frac{1}{2}\frac{(\ell+2)!}{(\ell-2)!}\right]^{-\frac{1}{2}}F_{\ell m\omega}. \tag{A4}$$

Here, $f = 1-2M/r$, and $A_{\ell m\omega}$, $A^{(1)}_{\ell m\omega}$, $B^{(0)}_{\ell m\omega}$, $B_{\ell m\omega}$, $\tilde{B}_{\ell m\omega}$, and $F_{\ell m\omega}$ are the Fourier-domain projections of the particle's energy-momentum tensor onto the tensor harmonic basis; cf. Ref. [32], Table I, for their expressions in time-domain and generic orbit. These functions encode information about the particle's geodesic motion, and when particularized for plunging geodesics they read

$$A_{\ell m\omega} = \mu\frac{V}{r^2 f^2}Y^*_{\ell m}e^{i\omega t_p}, \tag{A5a}$$

$$A^{(1)}_{\ell m\omega} = -i\sqrt{2}\mu\frac{\mathcal{E}}{r^2 f}Y^*_{\ell m}e^{i\omega t_p}, \tag{A5b}$$

$$B^{(0)}_{\ell m\omega} = i\mu\frac{\mathcal{E}\mathcal{L}}{Vr^3}\frac{1}{\sqrt{\ell(\ell+1)/2}}\partial_\phi Y^*_{\ell m}e^{i\omega t_p}, \tag{A5c}$$

$$B_{\ell m\omega} = -\mu\frac{\mathcal{L}}{r^3 f}\frac{1}{\sqrt{\ell(\ell+1)/2}}\partial_\phi Y^*_{\ell m}e^{i\omega t_p}, \tag{A5d}$$

$$F_{\ell m\omega} = \mu\frac{\mathcal{L}^2}{Vr^4}\left[\frac{1}{2}\frac{(\ell+2)!}{(\ell-2)!}\right]^{-\frac{1}{2}}\partial_{\phi\phi}Y^*_{\ell m}e^{i\omega t_p}, \tag{A5e}$$

where, for brevity, we wrote $Y^*_{\ell m} = Y^*_{\ell m}(\pi/2, \phi_p)$ and defined $V = \sqrt{\mathcal{E}^2 - U}$, where U is given by Eq. (3). Here, μ is the particle's mass and t_p and ϕ_p are functions of r, obtained by integrating the geodesic equation (5).

The source $S^{(-)}_{\ell m\omega}$, that excites the perturbations of axial parity, is given by

$$S^{(-)}_{\ell m\omega} = \frac{8\pi i f}{r}\left[\frac{1}{2}\frac{(\ell+2)!}{(\ell-2)!}\right]^{-\frac{1}{2}}\left[-r^2\frac{d}{dr}(fD_{\ell m\omega})\right.$$
$$\left. + \sqrt{2\lambda}rfQ_{\ell m\omega}\right], \tag{A6}$$

where, analogously to the polar case, $D_{\ell m\omega}$ and $Q_{\ell m\omega}$ are the Fourier-domain projections of the particle's energy-momentum tensor onto the tensor harmonic basis; cf. Ref. [32], Table I, for their time domain, general orbit forms. When particularized for plunging trajectories, $D_{\ell m\omega}$ and $Q_{\ell m\omega}$ become

$$D_{\ell m\omega} = i\mu\frac{\mathcal{L}^2}{Vr^4}\left[\frac{1}{2}\frac{(\ell+2)!}{(\ell-2)!}\right]^{-\frac{1}{2}}X^*_{\ell m}e^{i\omega t_p}, \tag{A7a}$$

$$Q_{\ell m\omega} = -i\mu\frac{\mathcal{L}}{fr^3}\frac{1}{\sqrt{\ell(\ell+1)/2}}\partial_\theta Y^*_{\ell m}e^{i\omega t_p}, \tag{A7b}$$

where we introduced the shorthand notation,

$$X_{\ell m} = 2\partial_\phi(\partial_\theta - \cot\theta)Y_{\ell m}. \tag{A8a}$$

In the case of radial infall, $\mathcal{L} = 0$, both $D_{\ell m\omega}$ and $Q_{\ell m\omega}$ are zero, and consequently $S^{(-)}_{\ell m\omega}$, vanishes.

APPENDIX B: THE NEAR-HORIZON AND FAR-FIELD EXPANSIONS OF THE REGGE-WHEELER AND ZERILLI FUNCTIONS

When integrating numerically the homogeneous Regge-Wheeler and Zerilli equations, we use series representations of the solutions to these equations in the near-horizon $[r/(2M) - 1 \ll 1$ or $x \to -\infty]$ and asymptotic ($r \gg 2M$ or $x \to \infty$) regions of the Schwarzschild spacetime. The coefficients in these series satisfy certain recursion relations that we summarize here.

We first consider the near-horizon limit. We assume that the Regge-Wheeler and Zerilli mode functions $X^{(\pm)}_{\ell m\omega}$ can be factorized as

$$X^{(\pm)}_{\ell m\omega} = e^{-i\omega x}\sum_{n=0}^{\infty}c_n^{(\pm)}z(r)^n, \qquad z = r/(2M) - 1. \tag{B1}$$

We substitute Eq. (B5) in the homogeneous equation (14) and derive a recursion relation between the coefficients $c_n^{(\pm)}$. For the Zerilli equation this relation is

$$\mathfrak{a}c_n^{(+)} = \mathfrak{b}c_{n-1}^{(+)} + \mathfrak{c}c_{n-2}^{(+)} + \mathfrak{d}c_{n-3}^{(+)} + \mathfrak{e}c_{n-4}^{(+)} + \mathfrak{f}c_{n-5}^{(+)}, \tag{B2}$$

where

$\mathfrak{a} = n(3 + 2\lambda)^2(n - 4i\sigma),$

$\mathfrak{b} = (3 + 2\lambda)\{4\lambda^2 + i(40\lambda + 36)(n - 1)\sigma + \lambda[2(9 - 4n)n - 6] - 3(n - 2)(2n - 1)\},$

$\mathfrak{c} = 24\lambda^3 - \lambda^2(24n^2 - 108n + 72) - \lambda(36n^2 - 168n + 174) - 9n^2 + i(160\lambda^2 + 288\lambda + 108)(n - 2)\sigma + 45n - 54,$

$\mathfrak{d} = 24\lambda^3 - \lambda^2(16n^2 - 108n + 144) - \lambda(12n^2 - 84n + 144) + i(160\lambda^2 + 192\lambda + 36)(n - 3)\sigma,$

$\mathfrak{e} = i\lambda(80\lambda + 48)(n - 4)\sigma - 4\lambda^2(n - 6)(n - 3) + 8\lambda^3,$

$\mathfrak{f} = 16i\lambda^2(n - 5)\sigma,$ \hfill (B3)

and $\sigma = M\omega$ [39]. For the Regge-Wheeler equation we obtain instead

$$n(n + 4i\sigma)c_n^{(-)} = -[2n^2 - 12i(n - 1)\sigma - 5n + \ell(\ell + 1) - 6]c_{n-1}^{(-)} - [(n - \ell - 3)(n + \ell - 2)$$
$$- 12i(n - 2)\sigma]c_{n-2}^{(-)} + 4i(n - 3)\sigma c_{n-3}^{(-)}. \tag{B4}$$

In Eqs. (B2) and (B4), $c_n^{(\pm)} = 0$ for negative values of n.

We now consider the asymptotic expansion of $X_{\ell m\omega}^{(\pm)}$. We assume they can be factorized as

$$X_{\ell m\omega}^{(\pm)} = J_{\ell m\omega}^{(\pm)}(r)e^{+i\omega x}, \tag{B5}$$

where $J_{\ell m\omega}^{(\pm)}$ ("Jost function") approaches a constant as $x \to \infty$ in order to recover a purely outgoing behavior. We then substitute Eq. (B5) in the homogeneous equation (14). This results in a differential equation for $J_{\ell m\omega}^{(\pm)}$,

$$\left[f\frac{d^2}{dr^2} + \left(\frac{2M}{r^2} + 2i\omega\right)\frac{d}{dr} - \frac{V_\ell^{(\pm)}}{f}\right]J_{\ell m\omega}^{(\pm)} = 0, \tag{B6}$$

which we solve with Frobenius' method. We assume a series expansion of the form,

$$J_{\ell m\omega}^{(\pm)} = \sum_{n=0}^{\infty} a_n^{(\pm)}/(\omega r)^n. \tag{B7}$$

We then substitute this expansion in Eq. (B6), and derive a recursion relation between the coefficients $a_n^{(\pm)}$. When using the Zerilli potential (11a), we obtain

$$2i\lambda^2 na_n^{(+)} = \lambda[\lambda(n - 1)n - 12i\sigma(n - 1) - 2\lambda(\lambda + 1)]a_{n-1}^{(+)}$$
$$+ 2\sigma[\lambda(3 - \lambda)(n - 2)(n - 1) - (\lambda^2 + 9i\sigma)$$
$$\times (n - 2) - 3\lambda^2]a_{n-2}^{(+)} + 3\sigma^2[(3 - 4\lambda)(n - 3)]$$
$$\times (n - 2) - 4\lambda(n - 3) - 6\lambda]a_{n-3}^{(+)}$$
$$- 18\sigma^3(n - 3)^2 a_{n-4}^{(+)}, \tag{B8}$$

while using the Regge-Wheeler potential (11b) we find

$$2ina_n^{(-)} = -2\sigma[(n + 1)(n - 3)]a_{n-1}^{(-)}$$
$$- [\ell(\ell + 1) - n(n - 1)]a_{n-2}^{(-)}, \tag{B9}$$

where $a_n^{(\pm)} = 0$ for negative values of n [34,60]. The derivations we just made also apply to modes that behave as $\simeq \exp(-i\omega x)$ at spatial infinity. In practice, we can replace $\sigma \to -\sigma$ in Eqs. (B8) and (B9).

APPENDIX C: CALCULATION OF THE WRONSKIAN

To calculate the Wronskian (23), we need first to calculate the mode amplitude $A_{\ell m\omega}^{(\pm)\text{in}}$. We do this calculation following the same strategy outlined in Ref. [29], Appendix A1, in the context of the Sasaki-Nakamura formalism.

We first integrate $X_{\ell m\omega}^{(\pm),\text{in}}$ from near the horizon [making use of the recursion relations (B2) and (B4)] out to some large $r_{\max}$. This gives us two constants $X_{\ell m\omega}^{(\pm),\text{in}}(r_{\max})$ and $dX_{\ell m\omega}^{(\pm),\text{in}}(r_{\max})/dr$. For large r, the mode function is approximately given by

$$X_{\ell m\omega}^{(\pm),\text{in}} \simeq A_{\ell m\omega}^{(\pm),\text{in}}e^{-i\omega x} + A_{\ell m\omega}^{(\pm),\text{out}}e^{+i\omega x},$$
$$= A_{\ell m\omega}^{(\pm),\text{in}}J_{\ell m\omega}^{(\pm),\text{in}}e^{-i\omega x} + A_{\ell m\omega}^{(\pm),\text{out}}J_{\ell m\omega}^{(\pm),\text{out}}e^{+i\omega x}, \tag{C1}$$

where we used the factorization (B5) in the second line.

We evaluate the Jost functions $J_{\ell m\omega}^{(\pm)}$ using the recursion relations (B8) and (B9), with $a_0^{(\pm)} = 1$ and adding terms in the series until a sufficient level of accuracy is reached. Equation (C1) and its derivative with respect to r provide two equations that depend on $X_{\ell m\omega}^{(\pm),\text{in}}$ (and its derivative) at $r_{\max}$; the outcomes of the numerical integration of $X_{\ell m\omega}^{(\pm),\text{in}}$. We use these two equations to solve for the two amplitudes $A_{\ell m\omega}^{(\pm),\text{in}}$ and $A_{\ell m\omega}^{(\pm),\text{out}}$. The former is then used to calculate the Wronskian (23).

[1] M. Rees, R. Ruffini, and J. A. Wheeler, *Black Holes, Gravitational Waves and Cosmology: An Introduction to Current Research* (Gordon and Breach, Science Publishers, Inc., New York, 1974).

[2] *Proceedings, Sources of Gravitational Radiation: Seattle, WA, USA, 1978*, edited by L. L. Smarr (Cambridge University Press, Cambridge, England, 1979).

[3] T. Regge and J. A. Wheeler, Stability of a Schwarzschild singularity, Phys. Rev. **108**, 1063 (1957).

[4] F. J. Zerilli, Effective potential for even-parity Regge-Wheeler gravitational perturbation equations, Phys. Rev. Lett. **24**, 737 (1970).

[5] F. J. Zerilli, Gravitational field of a particle falling in a Schwarzschild geometry analyzed in tensor harmonics, Phys. Rev. D **2**, 2141 (1970).

[6] M. Davis, R. Ruffini, W. H. Press, and R. H. Price, Gravitational radiation from a particle falling radially into a Schwarzschild black hole, Phys. Rev. Lett. **27**, 1466 (1971).

[7] M. Davis and R. Ruffini, Gravitational radiation in the presence of a Schwarzschild black hole. A boundary value search, Lett. Nuovo Cimento **2S2**, 1165 (1971).

[8] M. Davis, R. Ruffini, and J. Tiomno, Pulses of gravitational radiation of a particle falling radially into a Schwarzschild black hole, Phys. Rev. D **5**, 2932 (1972).

[9] K. P. Chung, A four-dimensional Green's function approach to the calculation of gravitational radiation from a particle falling into a black hole, Nuovo Cimento Soc. Ital. Fis. **14B**, 293 (1973).

[10] R. Ruffini, Gravitational radiation from a mass projected into a Schwarzschild black hole, Phys. Rev. D **7**, 972 (1973).

[11] S. A. Teukolsky, Perturbations of a rotating black hole. 1. Fundamental equations for gravitational electromagnetic and neutrino field perturbations, Astrophys. J. **185**, 635 (1973).

[12] S. L. Detweiler and E. Szedenits, Black holes and gravitational waves. II. Trajectories plunging into a nonrotating hole, Astrophys. J. **231**, 211 (1979).

[13] Y. Tashiro and H. Ezawa, Gravitational radiation of a particle falling towards a black hole. I. The case of nonrotating black hole, Prog. Theor. Phys. **66**, 1612 (1981).

[14] E. Poisson, Gravitational radiation from infall into a black hole: Regularization of the Teukolsky equation, Phys. Rev. D **55**, 639 (1997).

[15] M. Campanelli and C. O. Lousto, Regularization of the Teukolsky equation for rotating black holes, Phys. Rev. D **56**, 6363 (1997).

[16] M. Sasaki and T. Nakamura, The Regge-Wheeler equation with sources for both even and odd parity perturbations of the Schwarzschild geometry, Phys. Lett. **87A**, 85 (1981).

[17] M. Sasaki and T. Nakamura, A class of new perturbation equations for the Kerr geometry, Phys. Lett. **89A**, 68 (1982).

[18] M. Sasaki and T. Nakamura, Gravitational radiation from a Kerr black hole. 1. Formulation and a method for numerical analysis, Prog. Theor. Phys. **67**, 1788 (1982).

[19] K. I. Oohara and T. Nakamura, Energy, momentum and angular momentum of gravitational radiation from a particle plunging into a nonrotating black hole, Phys. Lett. **94A**, 349 (1983).

[20] K. I. Oohara and T. Nakamura, Energy, momentum and angular momentum of gravitational waves induced by a particle plunging into a Schwarzschild black hole, Prog. Theor. Phys. **70**, 757 (1983).

[21] K. I. Oohara and T. Nakamura, Gravitational waves from a particle scattered by a Schwarzschild black hole, Prog. Theor. Phys. **71**, 91 (1984).

[22] Y. Kojima and T. Nakamura, Gravitational radiation from a particle with zero orbital angular momentum plunging into a Kerr black hole, Phys. Lett. **96A**, 335 (1983).

[23] Y. Kojima and T. Nakamura, Gravitational radiation by a particle with nonzero orbital angular momentum falling into a Kerr black hole, Phys. Lett. **99A**, 37 (1983).

[24] M. Sasaki and T. Nakamura, Gravitational radiation from extreme Kerr black hole, Gen. Relativ. Gravit. **22**, 1351 (1990).

[25] C. T. Cunningham, R. H. Price, and V. Moncrief, Radiation from collapsing relativistic stars. I—Linearized odd-parity radiation, Astrophys. J. **224**, 643 (1978).

[26] V. Moncrief, Gravitational perturbations of spherically symmetric systems. I. The exterior problem, Ann. Phys. (N.Y.) **88**, 323 (1974).

[27] S. Hopper and V. Cardoso, Scattering of point particles by black holes: Gravitational radiation, Phys. Rev. D **97**, 044031 (2018).

[28] M. Shibata and T. Nakamura, Metric perturbations induced by a particle falling into a Schwarzschild black hole 1: Formulation, Prog. Theor. Phys. **87**, 1139 (1992).

[29] E. Berti, V. Cardoso, T. Hinderer, M. Lemos, F. Pretorius, U. Sperhake, and N. Yunes, Semianalytical estimates of scattering thresholds and gravitational radiation in ultrarelativistic black hole encounters, Phys. Rev. D **81**, 104048 (2010).

[30] R. Ruffini and M. Sasaki, On a semirelativistic treatment of the gravitational radiation from a mass thrusted into a black hole, Prog. Theor. Phys. **66**, 1627 (1981).

[31] E. Berti, V. Cardoso, L. Gualtieri, F. Pretorius, and U. Sperhake, Comment on "Kerr black holes as particle accelerators to arbitrarily high energy", Phys. Rev. Lett. **103**, 239001 (2009).

[32] N. Sago, H. Nakano, and M. Sasaki, Gauge problem in the gravitational self-force. 1. Harmonic gauge approach in the Schwarzschild background, Phys. Rev. D **67**, 104017 (2003).

[33] H. Nakano, N. Sago, and M. Sasaki, Gauge problem in the gravitational self-force. 2. First post-Newtonian force under Regge-Wheeler gauge, Phys. Rev. D **68**, 124003 (2003).

[34] S. Chandrasekhar and S. L. Detweiler, The quasi-normal modes of the Schwarzschild black hole, Proc. R. Soc. A **344**, 441 (1975).

[35] Black Hole Perturbation Toolkit, www.bhptoolkit.org.

[36] N. Warburton and B. Wardell, Applying the effective-source approach to frequency-domain self-force calculations, Phys. Rev. D **89**, 044046 (2014).

[37] B. Leather and N. Warburton, Applying the effective-source approach to frequency-domain self-force calculations for eccentric orbits, Phys. Rev. D **108**, 084045 (2023).

[38] S. Hopper, Unbound motion on a Schwarzschild background: Practical approaches to frequency domain computations, Phys. Rev. D **97**, 064007 (2018).

[39] S. Chandrasekhar, *The Mathematical Theory of Black Holes* (Oxford University Press, Oxford, 1985).

[40] E. W. Leaver, An analytic representation for the quasi normal modes of Kerr black holes, Proc. R. Soc. A **402**, 285 (1985).

[41] https://pages.jh.edu/eberti2/ringdown.

[42] W. H. Press, Long wave trains of gravitational waves from a vibrating black hole, Astrophys. J. Lett. **170**, L105 (1971).

[43] C. J. Goebel, Comments on the "vibrations" of a black hole, Astrophys. J. **172**, L95 (1972).

[44] V. Cardoso, A. S. Miranda, E. Berti, H. Witek, and V. T. Zanchin, Geodesic stability, Lyapunov exponents and quasinormal modes, Phys. Rev. D **79**, 064016 (2009).

[45] B. F. Schutz and C. M. Will, Black hole normal modes: A semianalytic approach, Astrophys. J. Lett. **291**, L33 (1985).

[46] S. Iyer and C. M. Will, Black hole normal modes: A WKB approach. 1. Foundations and application of a higher order WKB analysis of potential barrier scattering, Phys. Rev. D **35**, 3621 (1987).

[47] C. V. Vishveshwara, Scattering of gravitational radiation by a Schwarzschild black-hole, Nature (London) **227**, 936 (1970).

[48] S. Hadar, B. Kol, E. Berti, and V. Cardoso, Comparing numerical and analytical calculations of post-ISCO ringdown amplitudes, Phys. Rev. D **84**, 047501 (2011).

[49] A. Folacci and M. Ould El Hadj, Multipolar gravitational waveforms and ringdowns generated during the plunge from the innermost stable circular orbit into a Schwarzschild black hole, Phys. Rev. D **98**, 084008 (2018).

[50] S. Hadar and B. Kol, Post-ISCO ringdown amplitudes in extreme mass ratio inspiral, Phys. Rev. D **84**, 044019 (2011).

[51] C. Moreno-Garrido, E. Mediavilla, and J. Buitrago, Gravitational radiation from point masses in elliptical orbits: Spectral analysis and orbital parameters, Mon. Not. R. Astron. Soc. **274**, 115 (1995).

[52] K. Glampedakis, S. A. Hughes, and D. Kennefick, Approximating the inspiral of test bodies into Kerr black holes, Phys. Rev. D **66**, 064005 (2002).

[53] S. Babak, H. Fang, J. R. Gair, K. Glampedakis, and S. A. Hughes, "Kludge" gravitational waveforms for a test-body orbiting a Kerr black hole, Phys. Rev. D **75**, 024005 (2007); **77**, 04990(E) (2008).

[54] M. Maggiore, *Gravitational Waves: Volume 1: Theory and Experiments* (Oxford University Press, Oxford, 2007).

[55] V. Ferrari and R. Ruffini, On the structure of gravitational wave bursts: Implosion with finite kinetic energy, Phys. Lett. **98B**, 381 (1981).

[56] A. Borrelli, Gravitational radiation emitted when a mass falls onto a compact star, Nuovo Cimento Soc. Ital. Fis. **112B**, 225 (1997), https://www.sif.it/riviste/sif/ncb/econtents/1997/112/02-03/article/27.

[57] V. Ferrari, L. Gualtieri, and A. Borrelli, Stellar pulsations excited by a scattered mass, Phys. Rev. D **59**, 124020 (1999).

[58] K. Tominaga, M. Saijo, and K.-i. Maeda, Gravitational waves from a test particle scattered by a neutron star: Axial mode case, Phys. Rev. D **60**, 024004 (1999).

[59] J. Ruoff, P. Laguna, and J. Pullin, Excitation of neutron star oscillations by an orbiting particle, Phys. Rev. D **63**, 064019 (2001).

[60] S. Hopper and C. R. Evans, Gravitational perturbations and metric reconstruction: Method of extended homogeneous solutions applied to eccentric orbits on a Schwarzschild black hole, Phys. Rev. D **82**, 084010 (2010).